Observations of smoke-influenced aerosol during the Yosemite Aerosol Characterization Study: Size distributions and chemical composition

G. R. McMeeking, S. M. Kreidenweis, C. M. Carrico, T. Lee, and J. L. Collett Jr.
Department of Atmospheric Science, Colorado State University, Fort Collins, Colorado, USA

W. C. Malm
Cooperative Institute for Research in the Atmosphere, Colorado State University, Fort Collins, Colorado, USA

Received 25 August 2004; revised 14 February 2005; accepted 25 February 2005; published 11 May 2005.

[1] The Yosemite Aerosol Characterization Study (YACS) took place in Yosemite National Park from 15 July to 5 September 2002, during which time air masses arriving at the site were believed to have been influenced by smoke from numerous wildfires active in the western United States. Physical, optical, and chemical aerosol measurements were made to characterize visibility and to help define aerosol sources contributing to haze in the park, with a particular emphasis on the role of prescribed and wild fires. Measurements of dry aerosol size distributions were made with a differential mobility analyzer (DMA) and an optical particle counter (OPC). An iterative alignment method assuming a range of refractive indices was applied to OPC size distributions to match them to DMA size distributions, returning the real refractive index that yielded the best fit and generating a complete size distribution for $0.04 < D_p < 2$ μm. Retrieved dry aerosol real refractive indices generally ranged from 1.56 to 1.59 and were comparable to values estimated from composition measurements. Organic carbon was the dominant aerosol species during the study, particularly during periods identified as smoke impacted. Mie theory was used to determine mass scattering efficiencies (λ = 530 nm) from measured dry size distributions using retrieved refractive indices. These ranged from 3 to 6 $m^2\ g^{-1}$, with the highest values occurring during smoke-impacted episodes.

Citation: McMeeking, G. R., S. M. Kreidenweis, C. M. Carrico, T. Lee, J. L. Collett Jr., and W. C. Malm (2005), Observations of smoke-influenced aerosol during the Yosemite Aerosol Characterization Study: Size distributions and chemical composition, *J. Geophys. Res.*, *110*, D09206, doi:10.1029/2004JD005389.

1. Introduction

[2] The Yosemite Aerosol Characterization Study (YACS) was conducted from 15 July through 5 September 2002 in Yosemite National Park (YNP), California. The park is situated in the central Sierra Nevada in California. The chief goal of the study was to determine the influence of smoke from controlled burns and wildfires, both local and distant, on the physical, chemical and optical properties of aerosol sampled in the park.

[3] In 2001 the United States Environmental Protection Agency (EPA) established the Regional Haze Rule that mandates increasing emission controls to return national parks and wilderness areas to "natural visibility conditions" by the year 2064. For the last 16 years the Interagency Monitoring of Protected Visual Environments (IMPROVE) program has made measurements of visibility-reducing particles in federal Class I areas to determine the major factors affecting visibility in national parks and wilderness areas. These measurements show that for the western United States, home to a large number of national parks and wilderness areas, carbonaceous compounds (organic and elemental carbon) are the dominant aerosol species on an annual basis and are estimated to account for a significant fraction of the total light extinction [*Malm et al.*, 1994]. The sources and characteristics of these particles are difficult to determine with sufficient confidence necessary for the formulation of emission control policies. These difficulties are caused in part by the large variety of organic chemical species present in atmospheric particles and the poor understanding of the optical properties of these particles in the atmosphere [*Watson*, 2002]. A considerable amount of analytical effort is necessary for detailed characterization of aerosol organic fractions [*Sipin et al.*, 2003; *Jacobson et al.*, 2000; *Turpin et al.*, 2000]. Even comprehensive measurements of carbon-containing compounds typically identify a small fraction of the organic mass [*Brown et al.*, 2002; *Schauer et al.*, 2002, 2001; *Yu et al.*, 1998; *Rogge et*

0148-0227/05/2004JD005389$09.00

al., 1993]. Since analytical methods to determine total aerosol carbon do not identify compounds, assumptions for converting carbon concentrations to organic carbon aerosol mass concentrations must be used and have been shown to vary significantly for different locations [*Turpin and Lim*, 2001]. The size distributions, densities and refractive indices of carbonaceous particles are generally unknown. Considerable uncertainty is thus attached to values used to estimate light extinction from measurements of aerosol carbon mass concentrations.

[4] The presence of both natural and anthropogenic sources of carbonaceous aerosol in the United States, combined with the difficulty of easily distinguishing between the two with commonly used measurement techniques, makes determining the ''natural visibility conditions'' difficult, particularly in regions where carbonaceous particles are a significant fraction of the total aerosol. The EPA suggests default values for natural elemental carbon (EC) concentrations of 0.02 $\mu g\ m^{-3}$ and 0.47 $\mu g\ m^{-3}$ for natural organic carbon (OC) in the western United States. *Park et al.* [2003] used an emissions inventory to model EC and OC concentrations at several IMPROVE measurement sites. A simulation with climatological monthly mean fire emissions and a best estimate of biogenic OC sources was performed to estimate natural concentrations of carbonaceous aerosols in the United States. They estimated that natural EC and OC concentrations were 2–3 times higher than the recommended EPA default values for application to the Regional Haze Rule in most locations. This increase in background concentration translates to a decreased natural visibility on the order of 20% relative to EPA estimates [*Park et al.*, 2003]. It is not unreasonable to expect large fires to affect air quality in distant locations, making them regional rather than local sources of particles and trace gases. *Wotawa and Trainer* [2000] found that fires in western Canada influenced air quality in the southeast United States during a field study in 1995. Other studies observed long-range transport of fire smoke to the United States from Quebec and Central America [*Colarco et al.*, 2004; *Iziomon and Lohmann*, 2003; *Kreidenweis et al.*, 2001].

[5] Previous studies of the properties of aerosol particles emitted through biomass burning have usually focused on tropical regions because approximately 80% of global biomass burning emissions are in the tropics [*Hao and Liu*, 1994]. The Smoke, Clouds, and Radiation–Brazil (SCAR-B) field project involved measurements of surface biomass, fires, smoke aerosol and trace gases, clouds, and radiation over the Amazon in order to understand their climatic effects [*Kaufman et al.*, 1998]. The Southern Africa Regional Science Initiative (SAFARI) field campaign made similar measurements of biomass burning smoke aerosol and regional haze from savannah fires in Africa [*Haywood et al.*, 2003]. Recent smaller field studies have also examined the properties of particle emissions and their effects on cloud properties from tropical biomass burning in Asia as well as Africa and Central and Southern America [*Abel et al.*, 2003; *Ogunjobi et al.*, 2004; *Roberts et al.*, 2003]. The body of work on emissions by fires in nontropical locations is somewhat smaller. *Conny and Slater* [2002] examined EC and OC emitted by a controlled burn in a boreal region of Canada, while *Radke et al.* [1991] and *Martins et al.* [1996] investigated particle properties from biomass burning in the Pacific Northwest region of the United States. There remains a clear need for further characterization of the optical properties of regional haze that has been influenced by fire emissions [*Reid et al.*, 2005].

2. Method

[6] Measurements of aerosol physical, chemical and optical properties were made at Turtleback Dome in Yosemite National Park (119.70°W, 37.71°N, Elevation 1615 m). The park is located in the central region of the Sierra Nevada, approximately 200 km east of the city of San Francisco, California (see Figure 1). The measurement campaign took place between 15 July 2002 and 5 September 2002. Very little variation was seen in surface wind patterns during the study, with only occasional transport from the south and west, and almost no transport from east of the park.

[7] Aerosol size distributions were measured using two instruments in order to observe the size range $0.04 < D_p < 2\ \mu m$. A differential mobility analyzer (DMA, TSI Inc. Model 3081) operating with a condensation particle counter (CPC, TSI Inc. Model 3010) measured number concentration as a function of mobility diameter over the size range $0.04 < D_p < 0.85\ \mu m$. An optical particle counter (OPC, LASAIR 1003, Particle Measuring Systems) measured number concentration as a function of optical diameter over the size range $0.1 < D_p < 2\ \mu m$. Data from the two instruments were used to produce a complete size distribution in terms of a geometric diameter and thereby also retrieve particle refractive index [*Hand and Kreidenweis*, 2002]. The instruments were housed in an air-conditioned trailer and samples were drawn through an inlet in the roof. Particles were dried to approximately 10% relative humidity (RH) by passing the sample through a Perma Pure dryer (Perma Pure Inc.) to reduce uncertainties in particle sizing by the DMA due to variations in RH. An OPC sampled dried aerosol from the same inlet, however, failure of the instrument flow meter required replacing its data with measurements made by a second OPC not connected to the drying system. The RH in this second instrument was measured at the exhaust, and only data with RH <25% were used. Aerosol hygroscopic growth factors were observed to be very low through the study, so humidity effects on particle size were likely very small [*Carrico et al.*, 2005]. The study average RH for the exhaust flow of the OPC sampling nondried aerosol was $14 \pm 4\%$.

[8] Aerosol composition was determined by a number of measurements, which are discussed in detail by *Malm et al.* [2005]. A URG sampling system [*Lee et al.*, 2004] was used to collect particles on filter packs for ion chromatography (IC) analysis for major ions including: SO_4^{2-}, NO^{3-}, Cl^-, Na^+, K^+, Ca^{2+}, Mg^{2+}, NH_4^+ and oxalate. The set up consisted of a 2.5 μm cyclone, two denuders coated with Na_2CO_3 and H_3PO_3 to collect nitric acid and ammonia gas, respectively, a Teflon primary filter for particle collection, and a nylon backup filter to collect nitric acid volatilized from the primary filter. Samples were typically collected for 24 hours beginning at 0800 PST, though several 6 hour samples

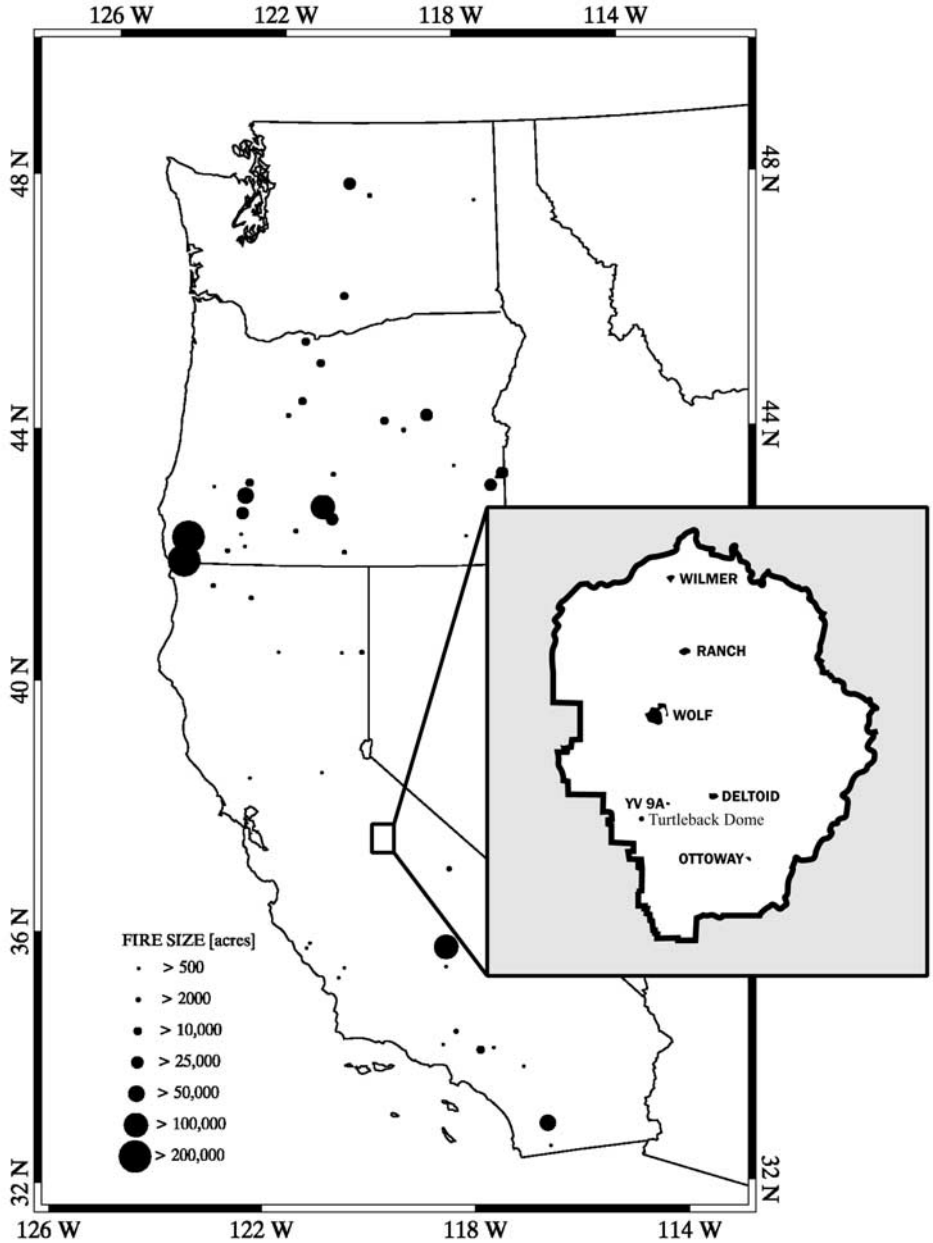

Figure 1. Map showing locations of fires (>500 acres) during the study in Washington, Oregon, and California, Yosemite National Park (small rectangle), and locations and names of selected fires within the park (inset).

were collected during intensive study periods. $PM_{2.5}$ (particles smaller than 2.5 μm aerodynamic diameter), organic carbon (OC) concentrations were obtained from an IMPROVE (Interagency Monitoring of Protected Visual Environments) sampler [*Malm et al.*, 1994], operating on the same sampling interval as the URG system, with the standard thermal optical reflectance (TOR) technique employed by the IMPROVE program. Black carbon (BC) concentrations were determined from 880 nm light absorption measured by a dual-wavelength aethalometer.

3. Aerosol Size Distributions

[9] For several days from 27 July 2002 through 5 August 2002, and again from 8 to 23 August 2002, aerosol properties changed substantially compared with other periods. These time periods were characterized by elevated concentrations of potassium ion (K^+) and enhanced ultraviolet light absorption in aerosol sampled at the site, which are both commonly used wood smoke identifiers [*Allen et al.*, 2004; *Andreae*, 1983]. In addition, analysis of air parcel trajectories using a backward trajectory model (Hybrid Single Particle Lagrangian Integrated Trajectory v 4.7) [*Draxler and Rolph*, 2003] indicated that transport during this time was primarily from active fire regions in southwestern and southern Oregon. These periods were identified as smoke-impacted regional haze episodes. Figure 1 shows locations of wildfires (area burned >500 acres) in California, Oregon and Washington that were active during the study period. Other, shorter-duration episodes also appeared to

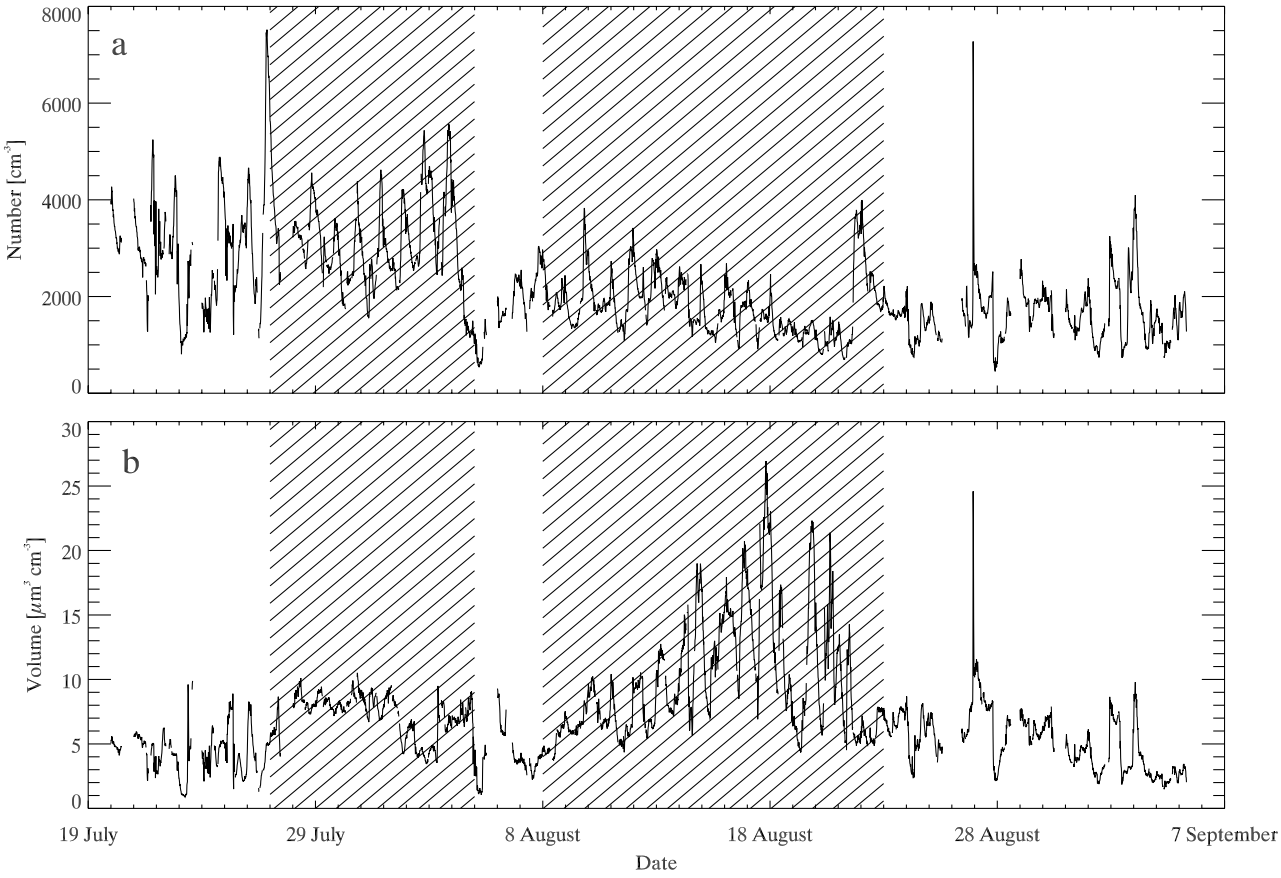

Figure 2. Integrated (a) number (cm^{-3}) and (b) volume (μm^3 μm^{-3}) concentrations calculated from measured dry size distributions. Hatching indicates periods with strong smoke-dominated regional haze influence.

have been considerably impacted by smoke. The locations of smaller fires within the park itself are shown in the inset, as is the location of the study site.

[10] Aerosol size distribution statistics were determined for dry merged size distributions for the size range $0.04 < D_p < 2$ μm following the procedure given by *Knutson and Lioy* [1989]. Volume and number distributions were described by 62 bins, each having a logarithmic bin width of 0.03 (base 10). The coarse mode was not fully captured by the instruments used in the alignment procedure, so statistics were performed for the accumulation mode only. The accumulation mode was defined by the minimum in the volume distribution between the two modes. The lower diameter limit of the accumulation mode was fixed at 0.04 μm and the upper limit was found through an automated routine that sought the minimum volume distribution value between $0.5 < D_p < 2$ μm. In cases where there was no obvious minimum in the volume distribution below 2 μm, the accumulation mode was assumed to extend to 2 μm. In general, particles with $1 < D_p < 2$ μm represented a very small fraction of the total particle number and volume concentrations.

[11] Uncertainties in the various parameters discussed below were calculated using the method of error propagation described by *Bevington and Robinson* [1992]. These were dominated by the uncertainty in the flow rate (±3%), taken as one standard deviation of the measured flow rates, and uncertainty in particle counts determined by Poisson statistics. Uncertainties in volume concentration and volume distribution derived parameters are due to uncertainties in particle number concentration and in diameter. The uncertainty in diameter for particles sampled by the DMA depends on the uncertainties in the measured sheath flow rate, assumed particle shape factor, and uncertainties in the charging efficiency and the applied voltage and was estimated to be roughly ±2%, consistent with the estimates reported by *Mikhailov et al.* [2004] and *Carrico et al.* [2005]. Uncertainty in the diameter of the particles sampled by the OPC depends on the uncertainty of the refractive index. *Hand* [2001] found that the estimated uncertainty in particle diameter due to variations in m led to $\Delta m/\Delta D_p \approx 0.6$ μm^{-1}. Uncertainty in particle number concentration, N, was approximately 6% throughout the measurement period and uncertainty in volume concentration, V, was roughly 7%.

[12] Particle number concentration was highest during the first 2 weeks of the observation period, reaching values as high as 7500 cm^{-3} (Figure 2a) and were lower, on the order of 1500 cm^{-3}, during the remainder of the study. In general, N peaked near 2000 PST and was lowest around midday. High concentrations of sub-100 nm particles were responsible for the high number concentrations during the first 2 weeks of the study. Number distributions became bimodal during the two regional smoke haze episodes, especially so for the second episode.

[13] Distinct periods of elevated accumulation mode V are evident during the two regional haze episodes as well

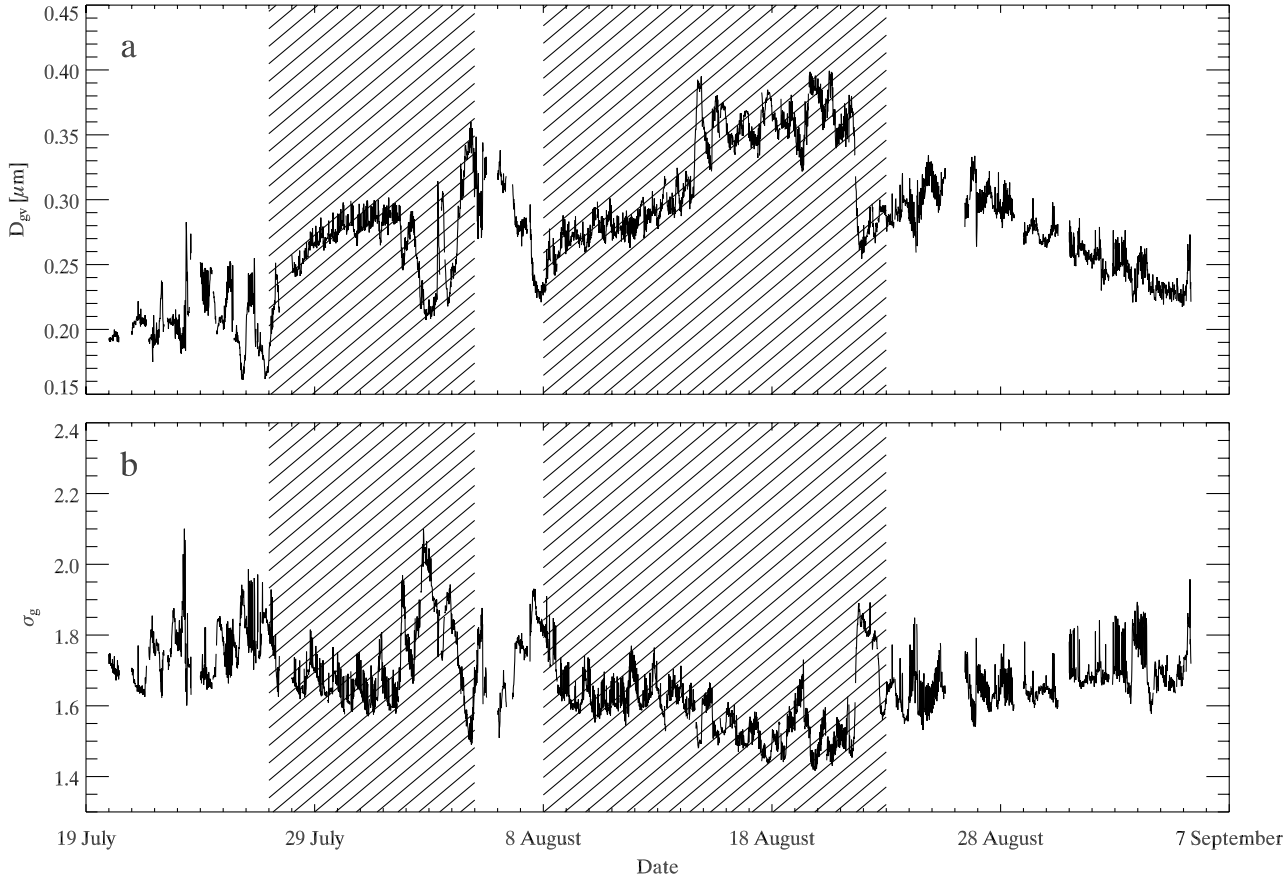

Figure 3. Accumulation mode volume mean (a) geometric diameter (μm) and (b) standard deviation from measured size distributions.

as a local smoke event on the evening of 26–27 August (Figure 2b). Relatively elevated volume concentrations were seen during time periods with possible local nighttime smoke influence during the time period 23–27 July. The overall mean and standard deviation of the accumulation mode volume concentration was 6.7 ± 3.9 $\mu m^3 cm^{-3}$ with highest values, during the second regional haze event, peaking at roughly 27 $\mu m^3 cm^{-3}$. The mean concentrations and one standard deviation during the first regional haze event was 7.9 ± 1.1 $\mu m^3 cm^{-3}$ and during the second regional haze event was 10.2 ± 4.6 $\mu m^3 cm^{-3}$. Volume concentrations were largest during the late afternoon/evening, from approximately 1500 PST to 0300 PST, though displaying a weaker daily pattern than seen for N.

[14] Accumulation mode volume mean geometric diameters (D_{gv}) were calculated from volume distributions (Figure 3a). The study average D_{gv} was 0.28 ± 0.05 μm. Large volume geometric mean diameters were observed during the second regional haze period, with values approaching 0.40 μm. The average D_{gv} was 0.32 ± 0.04 μm during this episode. Smaller values of D_{gv} were observed during the first week of the study, but displayed more variation during the period. Figure 3b shows accumulation mode volume geometric standard deviations (σ_g). The overall average was 1.67 ± 0.11, with largest values observed during the first half of the study and lowest values seen during the second regional haze episode. A strong relationship between σ_g and D_{gv} was seen, with the lowest standard deviations corresponding to higher mean diameters (Figure 4). This may reflect the aging of particles, which can result in increased particle size as mass is added and a narrowing of the standard deviation, seen in our data by an approach toward $\sigma_g \approx 1.5$, a value near the so-called "self-preserving size distribution" σ_g of 1.35 [*Hinds*, 1999]. *Reid et al.* [1998] reported similar observations for smoke-influenced hazes of varying ages in Brazil. Increasing D_{gv} also corresponded to increases in volume concentration (Figure 5).

[15] Regional haze episodes are clearly visible on a contour plot of volume distributions for the entire study (Figure 6), with high volume distribution values near 0.3–0.5 μm from 27 July 2004 to 3 August 2004 and 10–22 August 2004. The shift to larger diameters during the smoke haze episodes can be seen in the distributions. Volume distribution values above 1.0 μm are low except during the heaviest smoke haze periods (14–22 August 2004), although they are still much lower than the values below 1.0 μm. It is difficult to see the presence of the small tail of the coarse mode ($D_p \approx 1$–2 μm) in Figure 6 due to low instrument resolution.

4. Chemical Composition and Refractive Index Calculations

[16] Mass concentrations for the major $PM_{2.5}$ aerosol species obtained from filter measurements and continuously operating analyzers are presented in Figure 7. Data are presented either from 24 hour collection filter measurements

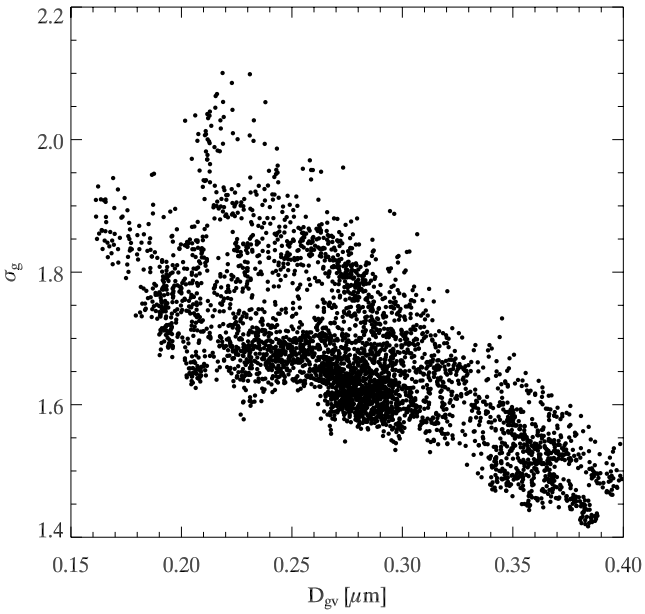

Figure 4. Accumulation mode volume mean geometric diameter (μm) versus standard deviation.

or, when data were obtained at higher time resolution, as 24 hour averages corresponding to the filter collection times. Organic mass concentration (OM) is OC concentration multiplied by an organic-molecular-mass-to-carbon-mass ratio of 1.8 to account for the mass of other molecular species present in the organic compounds [*Malm et al.*, 2005]. Highest organic mass concentrations were observed during regional haze episodes, reaching concentrations on the order of 20 μg m^{-3}. The composition of the ammoniated sulfate species was assumed to vary between ammonium sulfate ($(NH_4)_2SO_4$) and letovicite ($(NH_4)_3HSO_4$) depending on the molar ratio of ammonium and sulfate. Excess ammonia was assumed to be associated with nitrate in the form of ammonium nitrate (NH_4NO_3) and any remaining nitrate was assumed to be associated with sodium in the form of sodium nitrate ($NaNO_3$). Soil composition was reconstructed from IMPROVE elemental mass concentrations using the standard IMPROVE soil formula [*Malm et al.*, 1994]. Concentrations of inorganic species showed less variation in concentration than organic species during the study, indicating haze episodes were more associated with elevated carbonaceous aerosol concentrations. On average, organic carbon was the dominant $PM_{2.5}$ species during the study, with an average mass fraction of 64 ± 16%, reaching maximum values during regional haze episodes on the order of 85%. Ammoniated sulfate was the next most abundant species with an average mass fraction of 20 ± 10%, followed by soil at 7.1 ± 3.1% and BC at 2.9 ± 0.5%.

[17] We assume all components are internally mixed in the $PM_{2.5}$ fraction. Estimates of the complex index of refraction ($m = n - ki$) and density of $PM_{2.5}$ aerosol were calculated from composition measurements using the volume weighted method of *Ouimette and Flagan* [1982]:

$$m = \bar{\rho} \sum_i \frac{X_i n_i}{\rho_i} - \bar{\rho} \sum_i \frac{X_i k_i}{\rho_i} i \qquad (1)$$

with

$$\frac{1}{\bar{\rho}} = \sum_i \frac{X_i}{\rho_i}, \qquad (2)$$

where n_i and k_i are the real and imaginary parts of the refractive index for species i, respectively, ρ_i is the density of species i and X_i is the mass fraction. Values assumed for the densities and refractive indices of the various species used in the calculation are given in Table 1. Calculated refractive index and density were most sensitive to the properties assumed for OC as it was the dominant species during the study. The values given for the refractive index (1.55) and density (1.4 g cm^{-3}) of OC are based on detailed measurements of various organic species in urban areas, but have been applied in both urban and remote locations [*Dick et al.*, 2000; *Hand and Kreidenweis*, 2002; *Stelson*, 1990; *Turpin and Lim*, 2001; *Zhang et al.*, 1994]. We include BC in our refractive index with an assumed refractive index of 1.96–0.66*i* [*Seinfeld and Pandis*, 1998]. Mass concentrations estimated by multiplying the integrated volume distributions by the density computed with equation (2) for each day agreed well with mass concentrations determined by a gravimetric filter measurement (Figure 8; error bars represent one standard deviation).

[18] The refractive index retrieved from the alignment (m_{align}) is governed by aerosol composition in the DMA-OPC overlap region ($0.2 < D_p < 0.7$ μm), so it may not agree with the refractive index calculated using $PM_{2.5}$ composition (m_{comp}) if there is significant variation in the particle composition with particle size. Good agreement between the real component of m_{align} and the real component of m_{comp} was observed for the duration of the study (Figure 9). The mean and standard deviation of the real part of m_{align} was 1.577 ± 0.008 and for the real part of m_{comp} was 1.570 ± 0.006. Best agreement was found during the

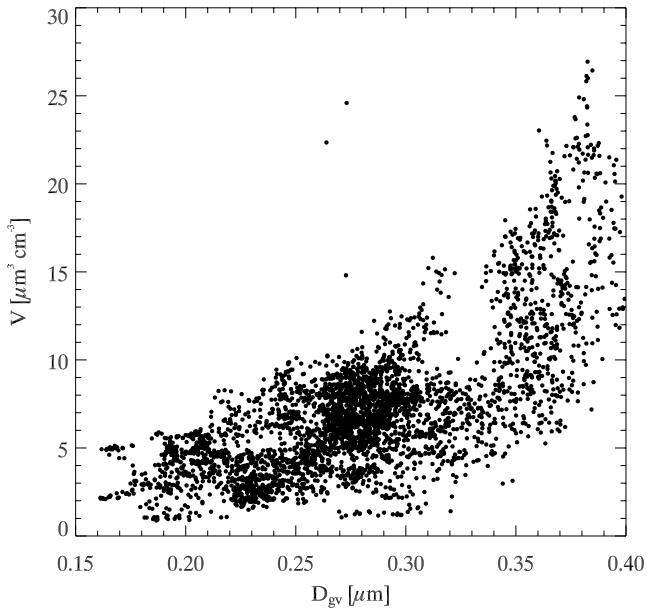

Figure 5. Accumulation mode volume mean geometric diameter (μm) versus integrated accumulation mode volume (μm^3 cm^{-3}) from dry size distributions.

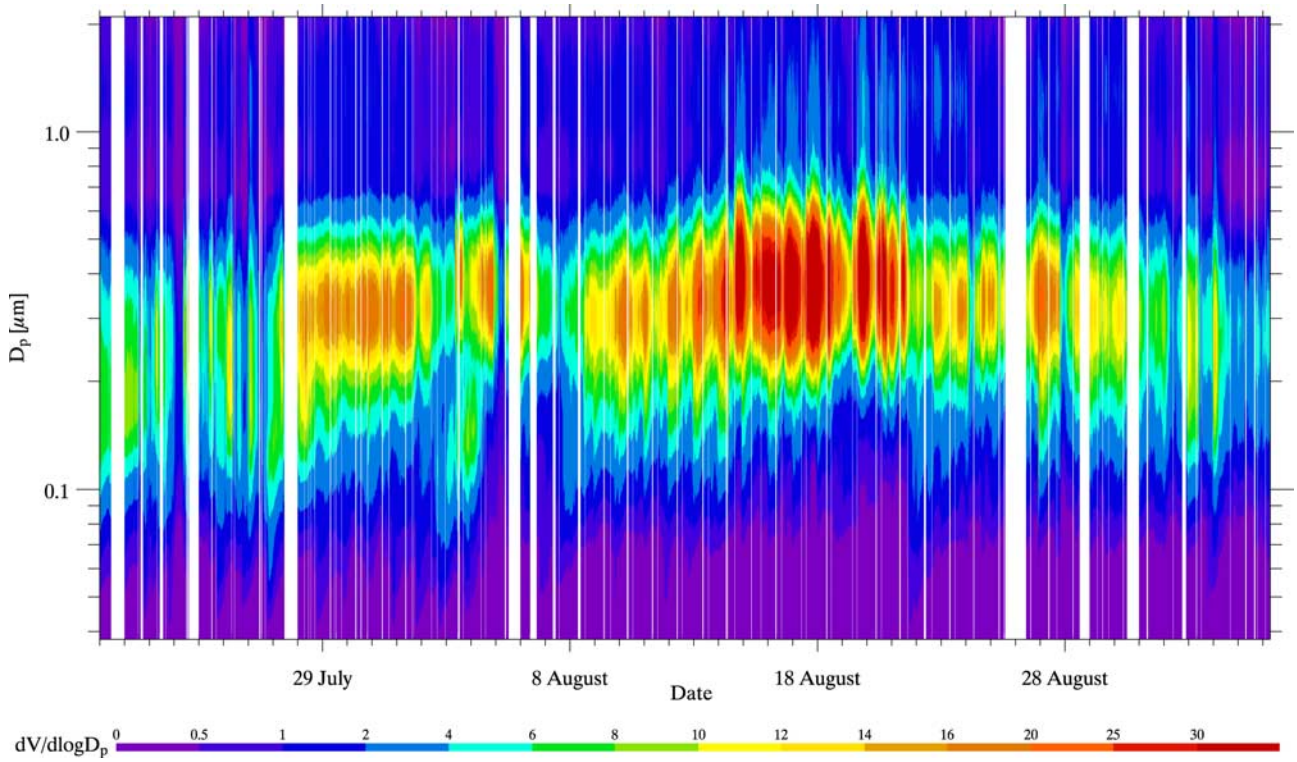

Figure 6. Contours of dry volume distributions (μm^3 cm^{-3}).

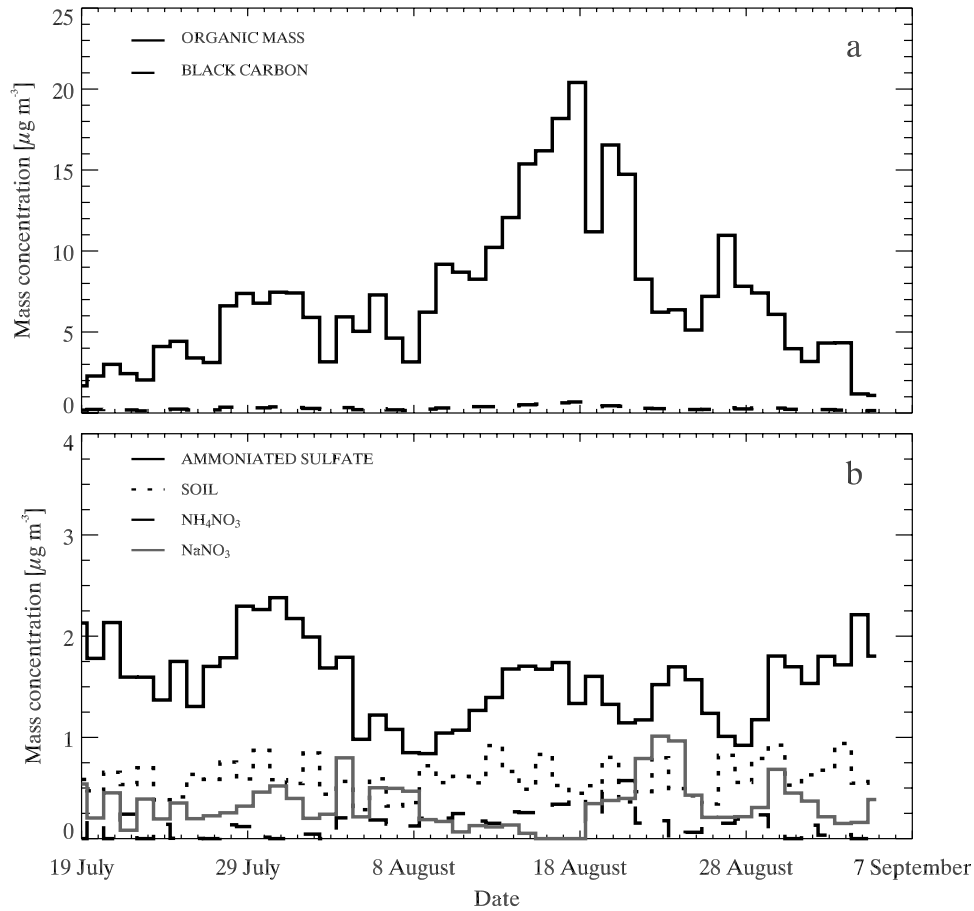

Figure 7. Fine ($PM_{2.5}$) mass concentrations (μg m^{-3}) of (a) carbonaceous aerosol and (b) major inorganic aerosol species.

Table 1. Physical Constants of Species Used to Calculate Refractive Index and Density

Species	Density, g cm^{-3}	Index of Refraction
$(NH_4)_3H(SO_4)_2$	1.83[a]	1.527[a]
$(NH_4)_2SO_4$	1.76[b]	1.531[b]
Organic carbon	1.4[c]	1.55[c]
Black carbon	2.0[d]	$1.96-0.66i$[d]
NH_4NO_3	1.725[e]	1.564[e]
$NaNO_3$	2.261[b]	1.587[b]
Soil	4[f]	2[f]

[a]From *Stelson* [1990].
[b]From *Tang* [1996].
[c]From *Dick et al.* [2000].
[d]From *Seinfeld and Pandis* [1998].
[e]From *Lide* [2000].
[f]Based on values reported by *Hand and Kreidenweis* [2002].

early and late periods of the study when OC concentrations were lowest. During carbon-dominated periods there is a bigger difference between the real parts of m_{align} and m_{comp}, but it is still small, 1–2%, within the experimental uncertainty. The larger differences during carbon-dominated periods suggest that the refractive index of 1.55 assumed for OC in the composition calculations was too low. Overall there was little variation in the real parts of both m_{align} or m_{comp}, reflecting the nearly continual presence of a dominant organic carbon mass fraction. The average imaginary part of m_{comp} was 0.015 ± 0.003 and highest values were observed during the early and late periods of the study, reflecting a larger contribution by BC to total $PM_{2.5}$ mass.

[19] *Yamasoe et al.* [1998] retrieved an "effective" real part of the complex refractive index of 1.533 ± 0.035 at λ = 438 nm and 1.553 ± 0.036 at λ = 670 nm for aged biomass burning hazes in Brazil using Sun/sky radiometer measurements. *Colarco et al.* [2004] report real components of 1.524 at λ = 440 nm and 1.554 at λ = 670 nm using a similar technique for a single measurement of an aged smoke plume over Washington D.C. thought to have originated over eastern Canada. Values determined during YACS are higher than these values. A likely source of this discrepancy is the presence of water on smoke haze aerosols observed by the radiometer, which would cause the "effective" refractive index to be lower than for dried smoke particles due to water's low refractive index (m = 1.33). *Wandinger et al.* [2002] inverted LIDAR (λ = 355, 400, 532, 710, 800, 1064 nm) measurements made in northern Europe of highly aged (approximately 6 days) biomass burning smoke from Canadian fires, to retrieve wavelength-independent refractive indices on the order of 1.65. The authors cite low relative humidity and the presence of iron oxide as the most likely reasons for the high refractive index values, and noted that decreasing relative humidity was correlated with higher refractive index values during their measurements. Refractive indices retrieved during YACS fall within the range of the reported values, and, given the uncertainty associated with the presence of water on aerosol particles, appear reasonable.

5. Mass Scattering Efficiency Calculations

[20] Mie theory can be used to calculate the scattering coefficient at a given wavelength for a known aerosol size distribution if the refractive index of the aerosol particles is known and they are assumed to be spherical. The real part of the refractive index used for the Mie calculations was the value retrieved by the alignment method (m_{align}) and was specific to each 15 min dry size distribution. The imaginary part of the refractive index was assigned the value of the imaginary component of the complex refractive index calculated for that day using equation (1) (m_{comp}). *Reid et al.* [2005] discuss issues associated with determining a physical model for the state of the aerosol mixture. Calculated scattering coefficients (λ = 530 nm) were divided by the size distribution-derived accumulation mode aerosol mass to determine mass scattering efficiencies (α_s) for each distribution sampled during the study (Figure 10). The average α_s during YACS was 4.3 ± 0.8 m^{2}g^{-1}, although this reflects varying degrees of influence by biomass burning aerosol throughout the course of the study. Highest values were found to occur in mid-August during the regional haze episode, with α_s approaching 6 m^{2}g^{-1}. This peak value is roughly 1.5 times higher than the value used for OC by the IMPROVE program to reconstruct dry aerosol scattering coefficients from filter composition measurements.

[21] Mass scattering efficiency can also be determined by dividing the scattering coefficient measured with a nephelometer by the aerosol mass measured on a filter. We performed this calculation using daily averaged scattering coefficients measured by a nephelometer sampling from a dried, 2.5 μm cutpoint inlet and the IMPROVE $PM_{2.5}$ gravimetric mass measured for each day [*Day and Malm*, 2001; *Malm et al.*, 1994]. The study average mass scattering efficiency determined using this method was 4.1 ± 0.7 m^{2}g^{-1} as compared to the size distribution based average of 4.3 ± 0.8 m^{2}g^{-1}. Mass scattering efficiencies

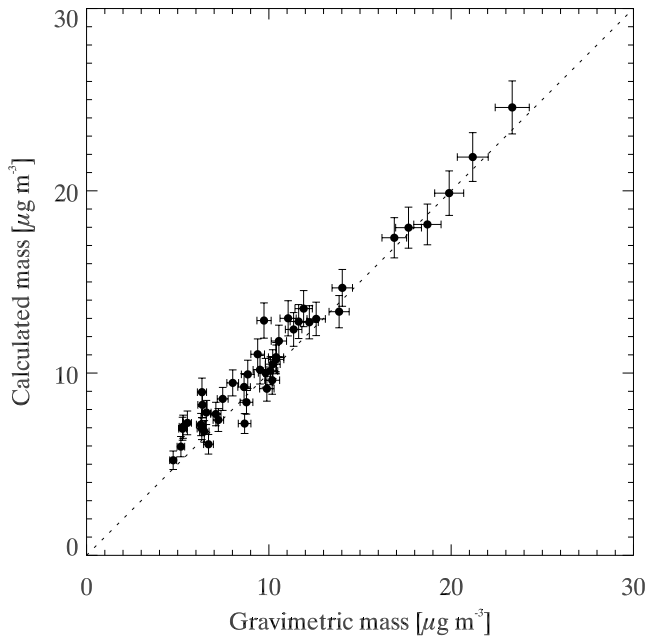

Figure 8. Relationship between gravimetric mass concentrations (abscissa) and mass concentrations (ordinate) calculated from integrated volume concentrations and density calculated from fine aerosol composition (μg m^{-3}). Error bars represent one standard deviation.

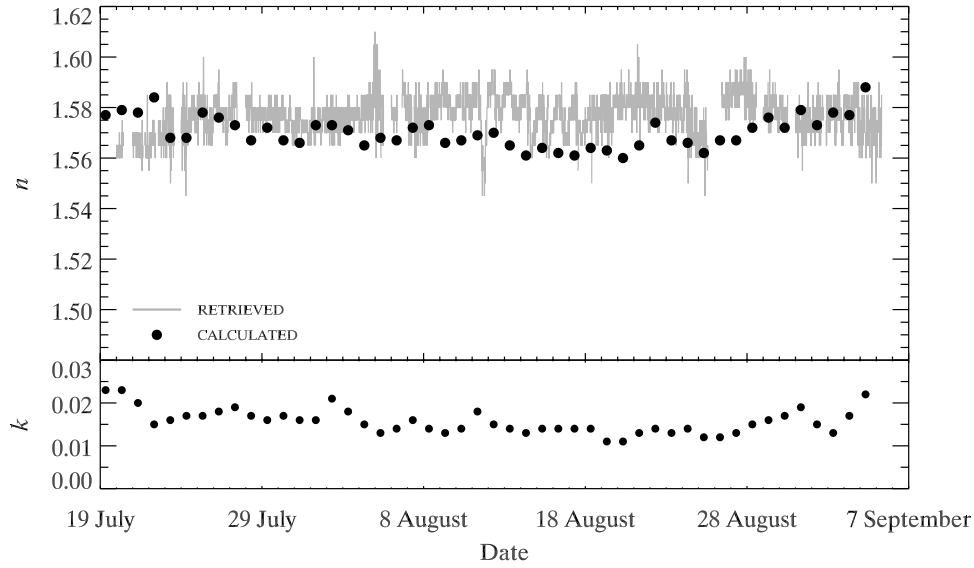

Figure 9. Retrieved dry refractive indices with computed real and imaginary components of the refractive index calculated from chemical composition of fine ($PM_{2.5}$) aerosol mass.

calculated in this way approached values as high as 6 m^2g^{-1}, similar to values determined from size distribution calculations. In general, both methods displayed similar trends with elevated values of the mass scattering efficiency occurring during smoke-impacted periods.

[22] Values of α_s observed during highly smoke-impacted regional haze episodes are more appropriate for comparisons with the aircraft based studies of tropical biomass burning regional hazes reported in Table 2. *Formenti et al.* [2003] estimated α_s to be 4.6 ± 0.8 m^2g^{-1} for aged smoke hazes off the coast of Namibia in southern Africa using aircraft-based nephelometer measurements of the dry scattering coefficient and mass reconstructed from submicron aerosol composition. *Haywood et al.* [2003] estimated an α_s of 4.6 ± 0.5 m^2g^{-1} by applying Mie theory to size distributions measured on the same aircraft. *Reid et al.* [1998] conducted aircraft-based measurements of particle size distributions, composition and scattering properties for biomass burning hazes over Brazil. Filters were gravimetrically analyzed in a humidity-controlled chamber (RH = 35%) to determine aerosol mass concentration. Nephelometer measurements were used to determine the scattering coefficient for aerosols dried to RH < 35%. Mass scattering efficiencies of aerosols sampled in a region thought to contain smoke on the order of 2–4 days old were 3.8 ± 0.8 m^2g^{-1}, were higher (4.1 ± 0.9 m^2g^{-1}) if soil was removed in the calculations, and increased as the smoke haze aged and grew into more effective light scattering sizes [*Reid et al.*, 1998]. *Reid et al.* [2005] summarize these and other reported values of α_s for fresh and aged smoke and suggest 4.3 ± 0.4 m^2g^{-1} as a likely α_s at 550 nm for temperate/boreal forest aged smoke.

6. Summary

[23] Several very large wildfires and numerous smaller fires occurred throughout the western United States during YACS, and haze impacted by smoke from these fires was observed at Yosemite National Park. Meteorological conditions suggested that fires burning in Oregon had the

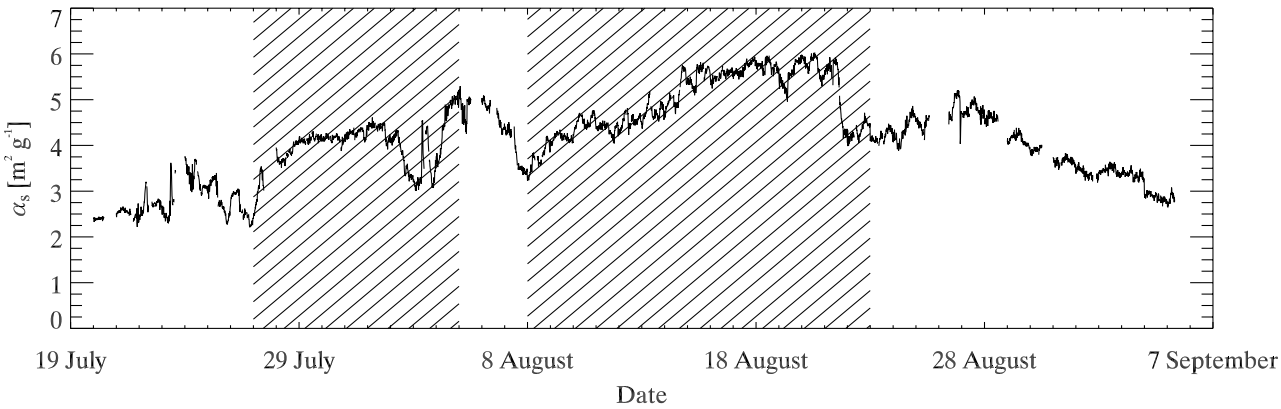

Figure 10. Dry mass scattering efficiencies (m^2 g^{-1}) calculated from volume distributions using retrieved real and calculated imaginary components of the refractive index and densities calculated from fine aerosol composition.

Table 2. Mass Scattering Efficiency for Biomass Burning Aerosol Measured in Several Different Locations From Selected Studies

Location	Platform	α_s, $m^2\ g^{-1}$	λ, nm
Western United States[a]	ground	5.5 ± 0.5 (estimate)	530
Southern Africa[b]	aircraft	4.6 ± 0.6	567
Southern Africa[c]	aircraft	4.6 ± 0.5	567
Brazil[d]	aircraft	4.1 ± 0.9	550

[a]This study.
[b]From *Formenti et al.* [2003].
[c]From *Haywood et al.* [2003].
[d]From *Reid et al.* [1998].

biggest impact on aerosol concentrations observed at the study site. Smoke-impacted haze episodes lasting several days occurred in late July and mid-August. Dry aerosol size distributions were measured using two instruments with different measurement ranges and techniques. An alignment method was used to reconcile data in the overlap region between the two instruments to produce a complete size distribution from 0.04 to 2 μm.

[24] Size distribution measurements showed that volume concentrations increased significantly during haze episodes. Size parameters derived from aerosol size distributions indicated that particles were larger during smoke haze episodes than during other times and had narrower distributions. Volume mean geometric diameters varied during the study with an overall average of 0.26 ± 0.05 μm, and D_{gv} was higher during two smoke-impacted regional haze periods, with an average value of 0.32 ± 0.04 μm. In general, aerosol distributions during smoke-impacted haze periods were characterized by larger volume concentrations, larger D_{gv} (as high as 0.4 μm) and narrower σ_g (≈1.5) than the study average. Little aerosol volume was observed at sizes greater than 1 μm, though the small upper size limit (≈2 μm) of the measurements presented in this work precludes conclusions being drawn about the contribution of coarse mode particles during YACS. Size distributions measured during smoke-impacted periods agreed well with size distributions measured for aged smoke in several other studies using various measurement platforms and instrumentation, considering uncertainties associated with type of biomass, the age of the haze and the effects of particle-borne water on optical properties.

[25] Aerosol composition was dominated by organic carbon for the majority of the study period, particularly during smoke-impacted haze episodes. Refractive indices calculated from aerosol composition (m_{comp}) were slightly lower than values retrieved using a size distribution alignment method (m_{align}), but agreed well within uncertainties in the optical properties of organic carbon. Overall, there was little variation with time in either calculated or retrieved refractive indices, reflecting relatively constant aerosol composition. Dry mass scattering efficiencies were determined from Mie theory estimates of scattering from dry size distributions and mass calculated by applying an estimated density to integrated dry volume distributions for the size range $0.04 < D_p < 2$ μm. High mass scattering efficiencies occurred during smoke-impacted haze episodes, reaching maximum values on the order of 6.0 $m^2 g^{-1}$, roughly 1.5 times the values used to reconstruct scattering using IMPROVE program methods for organic carbon and twice that used for common inorganic salts. This suggests that use of average mass scattering efficiencies in reconstructing aerosol extinction from mass concentrations leads to an underestimation of the impact of smoke from wildfires and controlled burns on visibility.

[26] **Acknowledgments.** The authors thank Air Resource Specialists and the Yosemite National Park staff for their assistance during the field study. We also thank the National Interagency Fire Center and K. Warner for national and park fire activity data. J. Carrillo provided data used for fire identification. We thank J. Hand for her assistance with the size distribution alignment process. The authors gratefully acknowledge the NOAA Air Resources Laboratory (ARL) for the provision of the HYSPLIT transport and dispersion model. Support for YACS-related work was provided by the National Park Service (contract CA2380-99001 TO0356).

References

Abel, S. J., J. M. Haywood, E. J. Highwood, J. Li, and P. R. Buseck (2003), Evolution of biomass burning aerosol properties from an agricultural fire in southern Africa, *Geophys. Res. Lett.*, *30*(15), 1783, doi:10.1029/2003GL017342.

Allen, G. A., P. Babich, and R. L. Poirot (2004), Evaluation of a new approach for real time assesment of wood smoke pm, paper presented at Regional and Global Perspectives on Haze: Causes, Consequences and Controversies—Visibility Specialty Conference, Am. Waste Manage. Assoc., Asheville, N. C., 25–29 Oct.

Andreae, M. O. (1983), Soot carbon and excess fine potassium: Long-range transport of combustion-derived aerosols, *Science*, *220*, 1148–1151.

Bevington, P., and D. Robinson (1992), *Data Reduction and Error Analysis for the Physical Sciences*, McGraw-Hill, New York.

Brown, S. G., P. Herckes, L. Ashbaugh, M. P. Hannigan, S. M. Kreidenweis, and J. J. L. Collett (2002), Characterization of organic aerosol in Big Bend National Park, Texas, *Atmos. Environ.*, *36*, 5807–5818.

Carrico, C. M., S. M. Kreidenweis, W. C. Malm, D. E. Day, T. Lee, J. Carrillo, G. R. McMeeking, and J. J. Collett Jr. (2005), Hygroscopic growth behavior of a carbon-dominated aerosol in Yosemite National Park, *Atmos. Environ.*, *39*, 1393–1404.

Colarco, P. R., M. R. Schoeberl, B. G. Doddridge, L. T. Marufu, O. Torres, and E. J. Welton (2004), Transport of smoke from Canadian forest fires to the surface near Washington, D. C.: Injection height, entrainment, and optical properties, *J. Geophys. Res.*, *109*, D06203, doi:10.1029/2003JD004248.

Conny, J. M., and J. F. Slater (2002), Black carbon and organic carbon in aerosol particles from crown fires in the Canadian boreal forest, *J. Geophys. Res.*, *107*(D11), 4116, doi:10.1029/2001JD001528.

Day, D. E., and W. C. Malm (2001), Aerosol light scattering measurements as a function of relative humidity: A comparison between measurements made at three different sites, *Atmos. Environ.*, *35*, 5169–5176.

Dick, W. D., P. Saxena, and P. H. McMurry (2000), Estimation of water uptake by organic compounds in submicron aerosols measured during the Southeastern Aerosol and Visibility Study, *J. Geophys. Res.*, *105*, 1471–1480.

Draxler, R. R., and G. D. Rolph (2003), Hysplit (HYbrid Single-Particle Lagrangian Integrated Trajectory) model access, report, NOAA Air Resour. Lab., Silver Spring, Md.

Formenti, P., W. Elbert, W. Maenhaut, J. Haywood, S. Osborne, and M. O. Andreae (2003), Inorganic and carbonaceous aerosols during the Southern African Regional Science Initiative (SAFARI 2000) experiment: Chemical characteristics, physical properties, and emission data for smoke from African biomass burning, *J. Geophys. Res.*, *108*(D13), 8488, doi:10.1029/2002JD002408.

Hand, J. L. (2001), A new technique for obtaining aerosol size distributions with applications to estimates of aerosol properties, Ph.D. thesis, Colo. State Univ., Fort Collins.

Hand, J. L., and S. M. Kreidenweis (2002), A new method for retrieving particle refractive index and effective density from aerosol size distribution data, *Aerosol Sci. Technol.*, *36*, 1012–1026.

Hao, W. M., and M. H. Liu (1994), Spatial and temporal distribution of tropical biomass burning, *Global Biogeochem. Cycles*, *8*, 495–503.

Haywood, J. M., S. R. Osborne, P. N. Francis, A. Keil, P. Formenti, M. O. Andreae, and P. H. Kaye (2003), The mean physical and optical properties of regional haze dominated by biomass burning aerosol measured from the C-130 aircraft during SAFARI 2000, *J. Geophys. Res.*, *108*(D13), 8473, doi:10.1029/2002JD002226.

Hinds, W. C. (1999), *Aerosol Technology*, 2nd ed., John Wiley, Hoboken, N. J.

Iziomon, M. G., and U. Lohmann (2003), Optical and meteorological properties of smoke-dominated haze at the ARM Southern Great

Plains Central Facility, *Geophys. Res. Lett.*, *30*(3), 1123, doi:10.1029/2002GL016606.

Jacobson, M. C., H.-C. Hansson, K. J. Noone, and R. J. Charlson (2000), Organic atmospheric aerosols: Review and state of the science, *Rev. Geophys.*, *38*, 267–294.

Kaufman, Y. J., et al. (1998), Smoke, Clouds, and Radiation–Brazil (SCAR-B) experiment, *J. Geophys. Res.*, *103*, 31,783–31,808.

Knutson, E. O., and P. J. Lioy (1989), Measurement and presentation of aersosol size distributions, in *Air Sampling Instruments for Evaluation of Atmospheric Contaminants*, 7th ed., edited by S. V. Hering, pp. 59–71, Am. Conf. of Govt. Indust. Hygienists, Cincinatti, Ohio.

Kreidenweis, S. M., L. A. Remer, R. Bruintjes, and O. Dubovik (2001), Smoke aerosol from biomass burning in Mexico: Hygroscopic smoke optical model, *J. Geophys. Res.*, *106*, 4831–4844.

Lee, T., S. M. Kreidenwels, and J. L. Collett (2004), Aerosol ion characteristics during the Big Bend Regional Aerosol and Visibility Observational Study, *J. Air Waste Manage. Assoc.*, *54*, 585–592.

Lide, D. R. (Ed.) (2000), *Handbook of Chemistry and Physics*, 83rd ed., CRC Press, Boca Raton, Fla.

Malm, W. C., J. F. Sisler, D. Huffman, R. A. Eldred, and T. A. Cahill (1994), Spatial and seasonal trends in particle concentration and optical extinction in the United States, *J. Geophys. Res.*, *99*, 1347–1370.

Malm, W. C., et al. (2005), Intercomparison and closure calculations using measurements of aerosol species and optical properties during the Yosemite Aerosol Characterization Study, *J. Geophys. Res.*, doi:10.1029/2004JD005494, in press.

Martins, J. V., P. Artaxo, P. V. Hobbs, C. Liousse, H. Cachier, Y. Kaufman, and A. Plana-Fattori (1996), Particle size distributions, elemental compositions, carbon measurements, and optical properties of smoke from biomass burning in the Pacific Northwest of the United States, in *Biomass Burning and Global Change*, edited by J. S. Levine, pp. 716–732, MIT Press, Cambridge, Mass.

Mikhailov, E., S. Vlasenko, R. Niessner, and U. Poschl (2004), Interaction of aerosol particles composed of protein and salts with water vapor: Hygroscopic growth and microstructural rearrangement, *Atmos. Chem. Phys.*, *4*, 323–350.

Ogunjobi, K. O., Z. He, K. W. Kim, and Y. J. Kim (2004), Aerosol optical depth during episodes of Asian dust storms and biomass burning at Kwangju, South Korea, *Atmos. Environ.*, *38*, 1313–1323.

Ouimette, J. R., and R. C. Flagan (1982), The extinction coefficient of multicomponent aerosols, *Atmos. Environ.*, *16*, 2405–2419.

Park, R. J., D. J. Jacob, M. Chin, and R. V. Martin (2003), Sources of carbonaceous aerosols over the United States and implications for natural visbility, *J. Geophys. Res.*, *108*(D12), 4355, doi:10.1029/2002JD003190.

Radke, R. J., D. A. Hegg, P. V. Hobbs, J. D. Nance, J. H. Lyons, K. K. Laursen, R. E. Weiss, P. J. Riggan, and D. E. Ward (1991), Particulate and trace gas emissions from large biomass fires in North America, in *Global Biomass Burning: Atmospheric, Climatic, and Biospheric Implications*, edited by R. Prinn, pp. 219–224, MIT Press, Cambridge, Mass.

Reid, J. S., P. V. Hobbs, R. J. Ferek, D. R. Blake, J. V. Martins, M. R. Dunlap, and C. Liousse (1998), Physical, chemical, and optical properties of regional hazes dominated by smoke in Brazil, *J. Geophys. Res.*, *103*, 32,059–32,080.

Reid, J. S., T. F. Eck, S. A. Christopher, R. Koppmann, O. Dubovik, D. P. Eleuterio, B. N. Holben, E. A. Reid, and J. Zhang (2005), A review of biomass burning emissions part III: Intensive optical properties of biomass burning particles, *Atmos. Chem. Phys.*, *5*, 827–849.

Roberts, G. C., A. Nenes, J. H. Seinfeld, and M. O. Andreae (2003), Impact of biomass burning on cloud properties in the Amazon Basin, *J. Geophys. Res.*, *108*(D2), 4062, doi:10.1029/2001JD000985.

Rogge, W. F., M. A. Mazurek, L. M. Hildemann, G. R. Cass, and B. R. T. Simoneit (1993), Quantification of urban organic aerosols at a molecular level: Identification, abundance, and seasonal variation, *Atmos. Environ.*, *27A*, 1308–1330.

Schauer, J. J., M. J. Kleeman, G. R. Cass, and B. R. T. Simoneit (2001), Measurements of emissions from air pollution sources. 3. c1-c29 organic compounds from fireplace combustion of wood, *Environ. Sci. Technol.*, *35*, 1716–1728.

Schauer, J. J., M. J. Kleeman, G. R. Cass, and B. R. T. Simoneit (2002), Measurements of emissions from air pollution sources. 5. c1-c32 organic compounds from gasoline powered motor vehicles, *Environ. Sci. Technol.*, *36*, 1169–1180.

Seinfeld, J. H., and S. N. Pandis (1998), *Atmospheric Chemistry and Physics*, John Wiley, Hoboken, N. J.

Sipin, M. F., S. A. Guazzotti, and K. A. Prather (2003), Recent advances and some remaining challenges in analytical chemistry of the atmosphere, *Analytical Chem.*, *75*, 2929–2940.

Stelson, A. W. (1990), Urban aerosol refractive-index prediction by partial molar refraction approach, *Environ. Sci. Technol.*, *24*, 1676–1679.

Tang, I. N. (1996), Chemical and size effects of hygroscopic aerosols on light scattering coefficients, *J. Geophys. Res.*, *101*, 19,245–19,250.

Turpin, B. J., and H. J. Lim (2001), Species contributions to PM2.5 mass concentrations: Revisiting common assumptions for estimating organic mass, *Aerosol Sci. Technol.*, *35*, 602–610.

Turpin, B. J., P. Saxena, and E. Andrews (2000), Measuring and simulating particulate organics in the atmosphere: Problems and prospects, *Atmos. Environ.*, *34*, 2983–3013.

Wandinger, U., et al. (2002), Optical and microphysical characterization of biomass-burning and industrial-pollution aerosols from multiwavelength lidar and aircraft measurements, *J. Geophys. Res.*, *107*(D21), 8125, doi:10.1029/2000JD000202.

Watson, J. G. (2002), Visibility: Science and regulation, *J. Air Waste Manage. Assoc.*, *52*, 628–713.

Wotawa, G., and M. Trainer (2000), The influence of Canadian forest fires on pollutant concentrations in the United States, *Science*, *288*, 324–328.

Yamasoe, M. A., Y. J. Kaufman, O. Dubovik, L. A. Remer, B. N. Holben, and P. Artaxo (1998), Retrieval of the real part of the refractive index of smoke particles from Sun/sky measurements during SCAR-B, *J. Geophys. Res.*, *103*, 31,893–31,902.

Yu, J., R. C. Flagan, and J. H. Seinfeld (1998), Identification of products containing -cooh, -oh and -c=o in atmospheric oxidation of hydrocarbons, *Environ. Sci. Technol.*, *32*, 2357–2370.

Zhang, X. Q., B. J. Turpin, P. H. Mcmurry, S. V. Hering, and M. R. Stolzenburg (1994), Mie theory evaluation of species contributions to 1990 wintertime visibility reduction in the Grand Canyon, *J. Air Waste Manage. Assoc.*, *44*, 153–162.

C. M. Carrico, J. L. Collett Jr., S. M. Kreidenweis, T. Lee, and G. R. McMeeking, Department of Atmospheric Science, Colorado State University, Fort Collins, CO 80523, USA. (carrico@lamar.colostate.edu; collett@lamar.colostate.edu; soniak@atmos.colostate.edu; thlee@lamar.colostate.edu; grm@lamar.colostate.edu)

W. C. Malm, Cooperative Institute for Research in the Atmosphere, Colorado State University, Fort Collins, CO 80523, USA. (malm@cira.colostate.edu)